Disparate temperature-dependent virus – host dynamics for SARS-CoV-2 and SARS-CoV in the human respiratory epithelium

Philip V'kovski[1,2*], Mitra Gultom[1,2,3,4*], Silvio Steiner[1,2,3*], Jenna Kelly[1,2*], Julie Russeil[5], Bastien Mangeat[6], Elisa Cora[6], Joern Pezoldt[5], Melle Holwerda[1,2,3,4], Annika Kratzel[1,2,3], Laura Laloli[3,4], Manon Wider[4], Jasmine Portmann [1,2], Thao Tran[1,2,3], Nadine Ebert[1,2], Hanspeter Stalder[1,2], , Rune Hartmann[7], Vincent Gardeux[5,8], Daniel Alpern[5,8], Bart Deplancke[5,8], Volker Thiel[1,2], Ronald Dijkman[1,2,4§]

[1] Institute of Virology and Immunology (IVI), Bern, Switzerland

[2] Department of Infectious Diseases and Pathobiology, Vetsuisse Faculty, University of Bern, Bern, Switzerland

[3] Graduate School for Biomedical Science, University of Bern, Bern, Switzerland

[4] Institute for Infectious Diseases, University of Bern, Bern, Switzerland

[5] Institute of Bioengineering, School of Life Sciences, École Polytechnique Fédérale de Lausanne (EPFL), Lausanne, Switzerland

[6] Gene Expression Core Facility (GECF), School of Life Sciences, École Polytechnique Fédérale de Lausanne (EPFL), Lausanne, Switzerland

[7] Department of Molecular Biology and Genetics, Aarhus University, Aarhus, Denmark

[8] Swiss Institute of Bioinformatics, Lausanne, Switzerland

*equal contribution

§corresponding author: Ronald Dijkman, email: ronald.dijkman@ifik.unibe.ch, phone: +41 31 664 07 83

Abstract: 215 words

Main text: 2965 words

Abstract

The human conductive respiratory tract spans a long anatomical distance and represents an important barrier to constrain invading respiratory pathogens. The disparate ambient temperatures found in the upper and lower respiratory tract have been demonstrated to influence the replication kinetics of common cold viruses as well as the associated host responses. Here, we employed the human airway epithelial cell (hAEC) culture model to investigate the impact of ambient temperatures found in the upper and lower respiratory tract, 33°C and 37°C, respectively, on the viral replication kinetics and host innate immune response dynamics during SARS-CoV-2 and SARS-CoV infections. Strikingly, SARS-CoV-2, in contrast to SARS-CoV, replicated more efficiently at temperatures encountered in the upper respiratory tract, and displayed higher sensitivity to type I and type III IFNs than SARS-CoV. Time-resolved transcriptome analysis highlighted a temperature-dependent induction of IFN-mediated antiviral response, whose amplitude inversely correlated with the replication kinetic efficiencies of both SARS-CoV-2 and SARS-CoV at temperatures found in the upper and lower respiratory tract. Altogether, these data reflect clinical features of SARS-CoV-2 and SARS-CoV and subsequently, their associated human-to-human transmission efficiencies. They provide crucial insights of the profound impact of ambient temperatures on viral replication and associated pivotal virus - host interaction dynamics. This knowledge can be exploited for the development of novel intervention strategies against SARS-CoV-2.

Introduction

In December 2019, a new zoonotic coronavirus emerged in Wuhan, Hubei Province, China, which is currently referred to as Severe Acute Respiratory Syndrome Coronavirus 2 (SARS-CoV-2), and is the etiological agent of Coronavirus Disease 2019 (COVID-19) [1–3]. The novel coronavirus has a close phylogenetic relationship with SARS-CoV, which emerged in China in 2002/2003 and led to over 8000 confirmed cases worldwide, including 800 deaths [4]. SARS-CoV-2 differs from SARS-CoV by only 380 amino acids over its entire 30 kb genome and retains a high level of conservation in the receptor binding motifs that interact with the human receptor angiotensin converting enzyme 2 (ACE2) [5]. Despite these similarities, there are currently over 2 million confirmed cases of SARS-CoV-2 worldwide, including more than 130'000 deaths [6]. Moreover, although the cell surface receptor ACE2 and the serine protease TMPRSS2 have been demonstrated to serve as entry determinants for both SARS-CoV and SARS-CoV-2 [2,7–9], an accumulating body of evidence showing dissimilar human-to-human transmission dynamics and clinical courses between SARS-CoV-2 and SARS-CoV strongly suggest the presence of different virus-host dynamics during viral infection in the human respiratory epithelium [10–15].

The human conductive respiratory tract is lined by a pseudostratified, ciliated, columnar epithelium with mucin-producing goblet cells and represents an important barrier to constrain invading pathogens. The anatomical distance between the upper and lower respiratory conductive tract, and their different ambient temperatures (32-33°C and 37°C, respectively [16,17]) have previously been shown to influence the replication kinetics of diverse respiratory viruses, such as rhinoviruses, influenza viruses and coronaviruses [18–22]. Moreover, the disparity in ambient temperature also affects virus – host immune response dynamics, and thus potential human-to-human transmission dynamics [23]. Interestingly, SARS-CoV-2 has been detected earlier after infection than SARS-CoV in upper respiratory tissues of infected patients [10,13,14,24,25], suggesting that transmission kinetics and host innate immune response dynamics might differ between SARS-CoV and SARS-CoV-2 infections.

Since viral load may reflect the dynamic interaction between viral replication and inhibition by cellular defence mechanisms, we employed the human airway epithelial cell (hAEC) culture model to investigate the influence of different incubation temperatures on the viral replication kinetics and host immune response dynamics of both SARS-CoV and SARS-CoV-2 infections. Our study revealed that SARS-CoV-2 replication improved in hAEC cultures incubated at 33°C rather than 37°C and resulted in higher titers than SARS-CoV, while both viruses replicated equally efficiently at 37°C. Pretreatment of hAEC cultures with exogenous type I and III interferon (IFN) at different temperatures revealed that SARS-CoV-2 is equally sensitive to both type I and III IFN than SARS-CoV, thereby exemplifying the relevance of potent innate immune responses. Importantly, a detailed temporal transcriptome analysis of infected hAEC cultures corroborated initial findings and uncovered characteristic innate immune response gene signatures relating to the viral replication efficiency of SARS-CoV and SARS-CoV-2 at different ambient temperatures. Altogether, these results provide the first in-depth fundamental insight on the virus-host innate immune response dynamics of SARS-CoV-2 and the closely phylogenetically-related SARS-CoV, and likely reflect the clinical characteristics and transmission efficiencies of both viruses.

Results

Replication kinetics of SARS-CoV-2 and SARS-CoV at 33°C and 37°C

To assess the influence of the temperature variations that occur along the human respiratory tract, and to model virus-host interaction dynamics in distinct anatomical regions, we maintained well-differentiated hAEC cultures at either 33°C or 37°C throughout the experiment. hAEC cultures represent a well-characterized *in vitro* model that morphologically and functionally recapitulate the epithelial lining of the human respiratory tract *in vivo*. hAEC cultures from three different human donors were inoculated with either SARS-CoV-2/München-1.1/2020/929 or SARS-CoV Frankfurt 1 isolates using a multiplicity of infection (MOI) of 0.1. The polarity of viral progeny release was monitored by collecting apical washes and basolateral medium in 24-hour intervals for a period of 96 hours. Since SARS-CoV-2 can be detected early after infection in the upper respiratory specimens of infected patients [14,24,25], we incubated virus-infected cultures at both 33°C and 37°C to mimic the ambient temperatures of the human upper and lower respiratory tract, respectively. At 37°C SARS-CoV and SARS-CoV-2 replicated equally efficiently for the first 48 hours, after which SARS-CoV showed, for 2 out of 3 donors, approximately 10-fold higher apically released viral progeny titers than SARS-CoV-2 (**Fig. 1a**). Interestingly, when assessing viral replication efficiency at 33°C rather than at 37°C, it was apparent that SARS-CoV-2 infection resulted in 100-fold higher titers released in the apical compartment. In contrast, SARS-CoV replication at 33°C was significantly impaired and delayed until 72 hours post-infection (hpi) (**Fig. 1b**). Since the directionality of viral progeny release is crucial for subsequent virus spread and overall disease outcome, we also assessed whether SARS-CoV-2 was released to the apical surface, basolateral surface, or bilaterally. Similar to what we and others have observed previously for all other human coronaviruses, SARS-CoV-2 was predominantly released to the luminal surface (**Supp. Fig 1a, b**) [26,27].

To assess whether the observed differential temperature-dependent replication efficiencies are a result of the number of cells infected by SARS-CoV or SARS-CoV-2, hAEC cultures were fixed at 96 hpi and processed for immunofluorescence analysis using antibodies directed against the SARS-CoV Nucleocapsid protein. Additionally, to discern potential preferential virus tropism to a distinct cell type, characteristic markers of the hAEC culture's architecture, such as the intercellular tight junctions (ZO-1) and the presence of cilia (β-tubulin IV), were also included. Microscopy investigations revealed that despite the more efficient replication kinetics of SARS-CoV-2 at 33°C, the overall fraction of SARS-CoV and SARS-CoV-2 infected cells at 33°C and 37°C are comparable (**Fig. 1c, d and Supp. Fig. 2a, b**). Notably, at 96 hpi the majority of SARS-CoV and SARS-CoV-2 antigen positive cells overlapped with the non-ciliated cell population (**Fig 1c, d**). We previously observed that SARS-CoV infects both non-ciliated and ciliated cell populations [26], however, given that other reports show that SARS-CoV primarily targets ciliated cells [28], we analysed the localization of the entry receptor, ACE2, and β-tubulin IV markers by microscopy. Immunofluorescence analysis revealed that ACE2 overlaps with both ciliated and non-ciliated cell populations in uninfected hAEC cultures (**Supp. Fig. 3a**). In line with this, analysis of mRNA expression in non-infected hAEC cultures using single-cell RNA-sequencing (scRNA-seq) confirmed that both ACE2 and TMPRSS2 mRNA are found in both secretory and ciliated cell populations (**Supp. Fig. 3b-d**) [29]. Combined these results demonstrate that despite their shared requirement on ACE2 and TMPRSS2 for entry into host cells, SARS-CoV and SARS-CoV-2 display strong temperature-dependent variation in replication kinetics in hAEC cultures, suggestive of host determinants intervening

during post-entry stages of the viral life cycle. Importantly, the significantly enhanced replication of SARS-CoV-2 at 33°C, likely supports the increased replication in the upper respiratory tract and transmissibility of SARS-CoV-2 compared to SARS-CoV.

Sensitivity of SARS-CoV-2 and SARS-CoV to IFN

The amount of viral progeny secreted from infected cells may reflect the dynamic interplay between viral replication and its inhibition by cellular defence mechanisms, such as by different types of interferon stimulated genes (ISGs). To examine whether the induction of ISGs differentially affects SARS-CoV and SARS-CoV-2 replication, hAEC cultures were pretreated with exogenous type I and III interferon (IFN), IFN-αA/D and IFN-λ3 respectively, for 18 hours prior to infection, at either 33°C or 37°C. Hereafter, the hAEC culture medium was replaced with IFN-free medium and cells were infected with SARS-CoV and SARS-CoV-2 at an MOI of 0.1, at 33°C or 37°C, for 72 hours. The titration of apically released virus revealed that at 37°C, SARS-CoV was less sensitive to type I IFN than to type III IFN, similar to previously reported observations (**Fig. 2a, 24 hpi**) [11]. At 33°C however, where its replication dynamics are delayed (**Fig. 1b**), SARS-CoV displayed a similar sensitivity to type I and III IFNs (**Fig. 2b**). In contrast, SARS-CoV-2 appeared equally sensitive to IFN-αA/D and IFN-λ3 at 37°C (**Fig. 2c**), while being notably less affected by IFN-αA/D than IFN-λ3 at 33°C (**Fig. 2d, 24 hpi**). Overall SARS-CoV-2 replication kinetics were more severely impaired by IFN pretreatment compared to SARS-CoV, especially in conditions where type III IFN pre-treatment and infections were performed at 33°C (**Fig. 2b, d**). The reduction of viral progeny titers in both IFN pretreatment conditions were corroborated by immunofluorescence analysis at 72 hpi. Viral antigens were no longer detected upon immunostaining of the type I or III IFN-treated hAEC cultures with anti-SARS-CoV Nucleocapsid protein antibodies (**Fig. 2e-f**). Altogether, these results suggest that the viral replication kinetics of both SARS-CoV and SARS-CoV-2 in the upper and lower airways are heavily dependent on innate immune responses elicited by Type I and III IFN, and that a potent IFN response can efficiently restrict viral replication of SARS-CoV-2 in primary well-differentiated hAEC cultures.

Host dynamics in SARS-CoV-2 and SARS-CoV infected hAEC cultures at 33°C and 37°C

The notable impact of incubation temperatures on SARS-CoV and SARS-CoV-2 replication kinetics (**Fig. 1**) and reduction in viral loads upon Type I and III IFN pretreatment (**Fig. 2**) prompted the assessment of host transcriptional responses dynamics to SARS-CoV and SARS-CoV-2 infections at 33°C and 37°C. Cellular RNA was extracted from hAEC cultures infected with either SARS-CoV or SARS-CoV-2 (MOI 0.1), as well as uninfected cultures at 24, 48, 72, and 96 hpi and used for transcriptomics analysis following Bulk RNA Barcoding and sequencing (BRB-seq) protocol [30]. Data from 3 different biological donors was used to perform pairwise comparisons of SARS-CoV or SARS-CoV-2 virus-infected to unexposed hAEC cultures at individual time points for each temperature. A total, 245 differential expressed genes (DEG, $Log_2FC \geq 1.5$, FDR ≤ 0.05) were identified across 16 experimental conditions in three biological replicates, represented by 139 unique genes (**Fig. 3a, b and Supp. Fig. 4a-b**). All DEGs were detected in SARS-CoV-2 virus-infected hAEC cultures, whereas no DEGs were identified for SARS-CoV (**Fig. 3a, b and Supp. Fig. 4a-b**). Hierarchical clustering of the SARS-CoV-2 DEGs uncovered that irrespective of temperature, the overlap between time points is

relatively low and most unique DEGs are found at 72 and 96 hpi. Interestingly, DEGs were identified as early as 48 hours at 37°C but not at 33°C (**Fig. 3b**). Comparisons of DEGs of the 72- and 96-hour time points from both temperatures identified a core group of nine common ISG-related genes; *IFI35*, *OASL*, *CMP2K*, *HELZ2*, *DDX60*, *MX1*, *IFI44L*, *ISG15* and *IFIT3*. Following the individual comparisons for SARS-CoV-2, we also performed pairwise comparison between SARS-CoV and SARS-CoV-2 to determine which genes were differentially expressed between these viruses. This revealed that irrespectively of temperature the most contrasting difference was observed at 72 hours (**Supp. Fig. 4c, d**).

To investigate the clustering results in more detail, we summarized the expression levels of the 139 unique DEGs among the 16 conditions (**Fig. 3c**). This revealed a distinct temporal and temperature-dependent profile in SARS-CoV-2-infected hAEC cultures, while this was less apparent in SARS-CoV-infected hAEC cultures. Annotation of the top 2 up- and downregulated DEGs among the 16 distinct host gene expression profiles identified the chemokines and cytokines *CXCL10*, *CXCL11*, *TNFSF13B*, and *CCL5*/*RANTES*, responsible for immune cell recruitment from the bloodstream to the site of infection, as well as the pathogen recognition receptor (PRR) *RIG-I/DDX58* and the interferon-inducible 2'-5'-oligoadenylate synthetase-like protein (*OASL*), as some of the most pronounced DEGs that all showed an earlier and higher expression level at 37°C compared to 33°C (**Fig. 3c**). To identify significantly enriched biological pathways over time at the different ambient temperatures, we performed pathway enrichment analyses on all unique DEGs detected in the comparison analyses for SARS-CoV-2. This illustrated a distinct temperature-dependent profile for diverse IFN and antiviral signalling pathways (**Fig. 3d**). The 43 unique genes associated with these enriched pathways, including *RIG-I/DDX58* and *OASL*, all displayed a clear temporal, temperature-dependent expression pattern that are inversely associated with the previously observed temperature-dependent viral kinetics difference for SARS-CoV-2 (**Fig. 3e, Fig. 1a, b, and Supp. Fig. 5**). Of note, the delayed SARS-CoV replication kinetics at 33°C coincides with the upregulation of the viral restriction factor *IFITM1* at 48 and 72 hours (**Fig. 3e, Fig. 1b**).

We previously observed, in the context of influenza A/H1N1 virus, that only a small fraction of infected cells produces IFN [31], and because the majority of detected DEGs during SARS-CoV-2 infection were genes induced downstream of the IFN pathway, we sought to assess the individual expression of type I and III IFN genes over time. Despite *IFNB1, IFNL1, IFNL2* and *IFNL3* not being detected as significantly upregulated in our aforementioned DEG analyses (**Fig. 3a-e**), their expression levels in SARS-CoV-2 infected hAEC cultures followed a similar temperature-dependent pattern as the ISGs highlighted in Figure 3e (**Fig. 3f**). In contrast, and in agreement with previous results (**Fig. 3a, e**), SARS-CoV infection only induced a minor elevation of *IFNL2* at 37°C (**Fig. 3f**), which correlated with the upregulation of the viral restriction factor *IFITM1* at 48 and 72 hours (**Fig 3c**). These results suggest that SARS-CoV infection triggers only mild IFN induction, and that similar to influenza A/H1N1 virus, type III IFNs have a more dominant roles in the antiviral defence [31].

Taken together, these results clearly demonstrate that SARS-CoV-2 and SARS-CoV induce disparate, virus specific and temperature-dependent host responses that inversely correlate with the previously observed dissimilar viral replication efficiencies at temperatures corresponding to the upper and lower respiratory tract. The majority of DEGs are related to the antiviral and pro-inflammatory

response, which is much more pronounced in SARS-CoV-2 rather than SARS-CoV virus-infection, and the early induction of these DEGs at 37°C coincides with the reduced replication of SARS-CoV-2 at temperatures corresponding to the lower respiratory epithelium.

Discussion

In the current study, we demonstrate that the ambient temperatures reminiscent of the conditions in the upper and lower respiratory tract have a profound influence on both viral replication and virus-host dynamics, particularly innate immune responses, during SARS-CoV and SARS-CoV-2 infection in human airway epithelial cells. Using an authentic *in vitro* model for the human respiratory epithelium we demonstrated that SARS-CoV-2, in contrast to SARS-CoV, replicated 100-fold more efficiently at temperatures encountered in the upper respiratory tract, while having similar amounts of Nucleocapsid-antigen positive cells. In addition, SARS-CoV-2 displayed a higher sensitivity to type I and type III IFNs than SARS-CoV upon exogenous pretreatment of hAEC cultures, thereby highlighting another crucial hallmark in addition to their disparate viral replication efficiencies. Importantly, temporal transcriptome analysis showed a temperature-dependent induction of the IFN-mediated antiviral and pro-inflammatory responses that inversely correlated with the observed replication kinetic efficiencies of both SARS-CoV and SARS-CoV-2 at temperatures found in the upper and lower respiratory tract. One of the most profound phenotypical characteristics of fulminant SARS-CoV-2 is the early replication in the upper respiratory tract of infected individuals, which might facilitate the high transmissibility of SARS-CoV-2 [14,24,25]. In contrast, SARS-CoV was shown to primarily replicate in the lower respiratory tract and efficient transmissibility occurred at later stages of the clinical course [10,12,13]. The data presented here contribute to the understanding of the disparate human-to-human transmission dynamics for both zoonotic coronaviruses and provide a framework to understand the parameters of the molecular basis of exacerbations induced by SARS-CoV-2 infection in predisposed individuals.

Although SARS-CoV-2 replication was strongly potentiated at 33°C, no noticeable differences as to the number of infected cells, was observed between SARS-CoV and SARS-CoV-2 infected cultures. Given that the viral S protein receptor binding motifs interacting with the human receptor ACE2 are highly conserved between the two viruses and that both SARS-CoV and SARS-CoV-2 displayed a similar cell tropism, the 380 amino acid dissimilarities distinguishing SARS-CoV-2 from SARS-CoV account for their differential replication efficiencies [2,7–9]. Another factor that may have influenced our results is the 29-nucleotide truncation in the *ORF8* gene of SARS-CoV Frankfurt-1, which was maintained in the SARS-CoV lineage that initiated the international spread of SARS-CoV. Indeed, Muth and colleagues demonstrated that an intact *ORF8* invoked 10-fold higher replication kinetics at 37°C in various cell culture models, including hAEC cultures [32]. Therefore, besides comparing the replication of different SARS-CoV *ORF8* variants at the temperature corresponding to the upper respiratory tract, it would be equally compelling to assess the phenotypic influence of similar truncations in the *ORF8* gene of SARS-CoV-2, especially since several SARS-CoV-2 isolates bearing a 382-nucleotide deletion truncating the *ORF8* gene have been detected [33]. Such SARS-CoV-2 *ORF8* variants can be readily engineered using the reverse genetic system recently established in our laboratory [34].

In our study, we report different temperature-dependent viral replication efficiencies for SARS-CoV and SARS-CoV-2, inversely associated with the amplitude of the innate immune response, albeit

with a more pronounced phenotype for SARS-CoV-2. Foxman and colleagues elegantly described, in an analogous model to the human AEC cultures and by using common cold viruses, that the PRR-mediated IFN response is influenced by temperature [23]. While this may also apply in the context of SARS-CoV-2 infections, it is likely that the efficient replication of SARS-CoV-2 and the concurrent expression of a plethora of known coronavirus antagonists of the antiviral response also play a crucial role herein [35–40]. Nonetheless, we demonstrate that SARS-CoV-2 is more sensitive to both type I and III IFN than SARS-CoV. These data are supported by Lokugamage and colleagues, where type I IFN pre-treatment in Vero cells resulted in a similar outcome [41], as well as the well-documented dominant antiviral role of type III IFN during virus infection in the respiratory epithelium [31,42,43]. IFN lambda therefore represents an attractive candidate for the development of intervention strategies against SARS-CoV-2 respiratory infections.

The findings reported here provide crucial insights of the profound impact of ambient temperatures on pivotal virus – host interactions. This work will probably stem additional functional *in vivo* studies delineating the efficacy of antiviral responses triggered by SARS-CoV and SARS-CoV-2 infections, as well as deciphering the influence of viral antagonists and physical conditions. Therefore, the disparate viral replication efficiencies and host responses at 33°C and 37°C provide important insights in the molecular basis of SARS-CoV-2 and should be exploited broadly to support clinical interventions in COVID-19 patients.

Material and methods

Cells and human airway epithelial cell (hAEC) cultures

Vero-E6 cells (kindly provided by Doreen Muth, Marcel Müller, and Christian Drosten, Charité, Berlin, Germany) were propagated in Dulbecco's Modified Eagle Medium-GlutaMAX supplemented with 1 mM sodium pyruvate, 10% (v/v) heat-inactivated fetal bovine serum (FBS), 100 mg/ml streptomycin, 100 IU/ml penicillin, 1% (w/v) non-essential amino acids and 15 mM HEPES (Gibco). Cells were maintained at 37°C in a humidified incubator with 5% CO_2.

Primary human tracheobronchial epithelial cells were isolated from patients (>18 years old) undergoing bronchoscopy or pulmonary resection at the Cantonal Hospital in St. Gallen, Switzerland, or Inselspital in Bern, Switzerland, in accordance with ethical approval (EKSG 11/044, EKSG 11/103, KEK-BE 302/2015, and KEK-BE 1571/2019). Isolation and culturing of primary material was performed as previously described [44]. Briefly, cryopreserved cells were thawed and expanded for one week in BEGM medium. After initial expansion phase, cells were transferred into in collagen type IV-coated porous inserts (6.5 mm radius insert, Costar) in 24-well plates. Cells were expanded for another 2-3 days in BEGM in a liquid-liquid state. Once the cells reached 90% confluency, the basolateral medium was exchanged for ALI medium and the apical medium was removed to allow for the establishment of the air-liquid-interface (ALI). Basolateral ALI medium was exchanged three times per week and apical side was washed with Hanks balanced salt solution (HBSS, Gibco) once a week, until the development of a fully differentiated epithelium (3-4 weeks), which was monitored by optical microscopy. Several modifications to the original protocol were used. The concentrations of hydrocortisone for both BEGM and ALI were increased to 0.48 µg/ml and BEGM was further supplemented with the inhibitors 1 µmol/L A83-01 (Tocris, Switzerland), 3 µmol/L isoproterenol (Abcam, Cambridge, United Kingdom) and 5

µmol/L Y27832 (Tocris, Switzerland). Basolateral ALI medium was exchanged three times per week and apical side was washed with hanks balanced salt solution (HBSS, Gibco) once a week. hAEC cultures were maintained at 37°C in a humidified incubator with 5% CO_2.

Viruses

SARS-CoV strain Frankfurt-1 [32,45] and SARS-CoV-2 (SARS-CoV-2/München-1.1/2020/929) [34] were kindly provided by Daniela Niemeyer, Marcel Müller, and Christian Drosten, and propagated and titrated on Vero-E6 cells.

Infection of hAEC cultures

Well-differentiated hAEC cultures were infected with 30,000 plaque-forming units (PFU) of either SARS-CoV or SARS-CoV-2. Viruses were diluted in Hanks balanced salt solution (HBSS, Gibco), inoculated on the apical side and incubated for 1 h at 33°C or 37°C. Afterwards, virus inoculum was removed, and the apical surface washed three times with HBSS, whereby the third wash was collected as the 1 hpi timepoint. The cells were incubated at the indicated temperatures in a humidified incubator with 5% CO_2. Released virus progeny were monitored every 24 h by incubating 100 µl of HBSS on the apical surface 10 min prior to the time point. The apical washes were collected, diluted 1:1 with virus transport medium (VTM), and stored at -80°C for later analysis. Basolateral medium was collected at each time point and stored at -80°C for later analysis. Fresh ALI medium was then added to the basolateral compartment. To analyze virus replication following interferon (IFN) exposure, hAEC cultures were pretreated with recombinant universal type I IFN (100 IU/ml; Sigma) or recombinant IFN-λ3 (100 ng/ml; [46]) for 18 h from the basolateral side, prior to infection and incubated at either 33°C or 37°C. As controls, untreated hAEC cultures were used. Shortly before infection with SARS-CoV and SARS-CoV-2, the basolateral medium containing type I or type III IFN was removed and replaced with medium without exogenous IFN.

Immunofluorescence analysis of infected hAECs

Well-differentiated hAEC cultures were fixed with 4% (v/v) neutral buffered formalin and processed as previously described [44]. Cells were permeabilized in PBS supplemented with 50 mM NH_4Cl, 0.1% (w/v) Saponin and 2% (w/v) Bovine Serum Albumine (CB). To detect SARS-CoV and SARS-CoV-2, hAEC cultures were immunostained with a rabbit polyclonal antibody against SARS-CoV nucleocapsid protein (Rockland, 200-401-A50), which also cross-react with SARS-CoV-2. Cell distribution of ACE2 were detected with a rabbit polyclonal antibody against ACE2 (ab15348, Abcam). Alexa Fluor® 488-labeled donkey anti-rabbit IgG (H + L) (Jackson Immunoresearch) was used as secondary antibody. Alexa Fluor® 647-labeled rabbit anti-β-tubulin IV (9F3, Cell Signaling Technology) and Alexa Fluor® 594-labeled mouse anti-ZO1 (1A12, Thermo Fisher Scientific) were used to visualize cilia and tight junctions, respectively. Antibodies were diluted in CB. All samples were counterstained using 4',6-diamidino-2-phenylindole (DAPI, Thermo Fisher Scientific) to visualize the nuclei. Samples were imaged on a DeltaVision Elite High-Resolution imaging system (GE Healthcare Life Sciences) equipped with 60x oil immersion objective (1.4 NA), by acquiring 200-300 nm z-stacks over the entire thickness of the sample. Images were deconvolved using the integrated softWoRx software. When indicated, images were

alternatively acquired using an EVOS FL Auto 2 Imaging System equipped with a 40x air objective. All images were processed using Fiji software packages [47]. Brightness and contrast were adjusted identically to their corresponding controls. Figures were assembled using the FigureJ plugin[48].

Titration of apical and basolateral compartments

Viruses released in the apical or basolateral compartments were titrated by plaque assay on Vero-E6 cells. Shortly, 1.7E5 cells/ml were seeded in 24-well plates one day prior to the titration and inoculated with 10–fold serial dilutions of virus solutions. Inoculums were removed 1.5 hpi and replaced with overlay medium consisting of DMEM supplemented with 1.2% Avicel (RC-581, FMC biopolymer), 5% heat-inactivated FBS, 50 mg/ml streptomycin and 50 IU/ml penicillin. Cells were incubated at 37 °C 5% CO_2 for 48 hours, fixed with 4% (v/v) neutral buffered formalin and stained with crystal violet.

Bulk RNA Barcoding and sequencing (BRB-seq)

Total cellular RNA from mock and virus-infected hAEC cultures was extracted with the NucleoMag RNA kit (Macherey-Nagel) according manufacturers guidelines on a Kingfisher Flex Purification system (Thermofisher). Total RNA concentration was quantified with QuantiFluor® RNA System (Promega) according manufactures guidelines on a Cytation 5 multimode reader (Biotek). A total of 100 ng of total cellular RNA was used for the generation of Bulk RNA Barcoding and sequencing (BRB-seq) libraries, and the subsequent sequencing on an Illumina NextSeq 500 platform was done as previously described at a depth of 3 – 4 million raw reads per sample [30]. The sequencing reads were demultiplexed using the BRB-seqTools suite [30], and were aligned against a concatenation of the human gene annotation of the human genome (hg38), SARS coronavirus Frankfurt 1 (AY291315) and SARS-CoV-2/Wuhan-Hu1/2020 (NC_045512) viral genomes using STAR and HTSeq for producing the count matrices. All downstream analyses were performed using R (version 3.6.1). Library normalization and expression differences between samples were quantified using the DESeq2 package, with a cut-off of fold change (FC) ≥ 1.5 and False Discovery Rate (FDR) ≤ 0.05. Pathway enrichment analysis and data visualization was performed with a variety of R-packages [49–51].

Single cell RNA sequencing

For the analysis of ACE2 and TMPRSS2 mRNA expression we reanalysed the previous obtained raw sequencing data [31]. The resulting unique molecule identifier (UMI) count matrix of each individual sample was pre-processed, filtered individually and merged in Seurat (v3.1). Data scaling, normalization and regressing out unwanted sources of variation (number of UMI's, mitochondrial content, cell cycle phase) was performed using integrated SCtransform option, followed by dimensional reduction using UMAP (Uniform Manifold Approximation and Projection) embedding. For cell type annotation, the resulting integrated dataset was used for unsupervised graph-based clustering to annotate the different cell types using both cluster-specific marker genes and well-known canonical marker genes to match identified clusters with specific cell types found in the respiratory epithelium, as previously described [31].

Statistical testing

Distribution testing was performed using Shapiro-Wilk normality test (>0.05), followed by computing the P value of the mean log10 PFU/ml at each timepoint between SARS-CoV and SARS-CoV-2 using a two-sided paired sample t test. Analyses were performed using R (version 3.6.1).

Acknowledgements

We gratefully thank the École Polytechnique Fédérale de Lausanne (EPFL) and the University of Bern for providing special authorization to conduct our research during the SARS-CoV-2 outbreak. We are grateful to Sabina Berezowska and Irene Ramos-Centeno (Institute of Pathology, University of Bern) for providing the tissues via the Tissue Bank Bern. This work was supported by the European Commission (Marie Sklodowska-Curie Innovative Training Network “HONOURS”; grant agreement No 721367), the Swiss National Science Foundation grants 179260, 160780, 173085, and the German Federal Ministry of Education and Research, project RAPID.

References

1. Li, Q. *et al.* Early Transmission Dynamics in Wuhan, China, of Novel Coronavirus–Infected Pneumonia. *N. Engl. J. Med.* (2020) doi:10.1056/nejmoa2001316.
2. Zhou, P. *et al.* A pneumonia outbreak associated with a new coronavirus of probable bat origin. *Nature* **579**, 270–273 (2020).
3. Coronaviridae Study Group of the International Committee on Taxonomy of Viruses. The species Severe acute respiratory syndrome-related coronavirus: classifying 2019-nCoV and naming it SARS-CoV-2. *Nat. Microbiol.* 1–9 (2020) doi:10.1038/s41564-020-0695-z.
4. WHO | Summary of probable SARS cases with onset of illness from 1 November 2002 to 31 July 2003. https://www.who.int/csr/sars/country/table2004_04_21/en/.
5. Wu, A. *et al.* Genome Composition and Divergence of the Novel Coronavirus (2019-nCoV) Originating in China. *Cell Host Microbe* **27**, 325–328 (2020).
6. *WHO - Coronavirus sitation report*. https://www.who.int/docs/default-source/coronaviruse/situation-reports/20200420-sitrep-91-covid-19.pdf.
7. Li, W. *et al.* Angiotensin-converting enzyme 2 is a functional receptor for the SARS coronavirus. *Nature* **426**, 450–454 (2003).
8. Glowacka, I. *et al.* Evidence that TMPRSS2 Activates the Severe Acute Respiratory Syndrome Coronavirus Spike Protein for Membrane Fusion and Reduces Viral Control by the Humoral Immune Response. *J. Virol.* **85**, 4122–4134 (2011).
9. Hoffmann, M. *et al.* SARS-CoV-2 Cell Entry Depends on ACE2 and TMPRSS2 and Is Blocked by a Clinically Proven Protease Inhibitor. *Cell* (2020) doi:10.1016/j.cell.2020.02.052.
10. Cheng, P. K. C. *et al.* Viral shedding patterns of coronavirus in patients with probable severe acute respiratory syndrome. *Lancet* **363**, 1699–1700 (2004).
11. Peiris, J. S. M. *et al.* Coronavirus as a possible cause of severe acute respiratory syndrome. *Lancet* **361**, 1319–1325 (2003).
12. Peiris, J. S. M. *et al.* Clinical progression and viral load in a community outbreak of coronavirus-associated SARS pneumonia: A prospective study. *Lancet* **361**, 1767–1772 (2003).
13. Hung, I. F. N. *et al.* Viral loads in clinical specimens and SARS manifestations. *Emerg. Infect. Dis.* **10**, 1550–7 (2004).
14. Wölfel, R. *et al.* Virological assessment of hospitalized patients with COVID-2019. *Nature* 1–10

(2020) doi:10.1038/s41586-020-2196-x.

15. Zhou, F. *et al.* Clinical course and risk factors for mortality of adult inpatients with COVID-19 in Wuhan, China: a retrospective cohort study. *Lancet* **395**, 1054–1062 (2020).

16. McFadden, E. R. *et al.* Thermal mapping of the airways in humans. *J. Appl. Physiol.* **58**, 564–570 (1985).

17. Lindemann, J., Leiacker, R., Rettinger, G. & Keck, T. Nasal mucosal temperature during respiration. *Clin. Otolaryngol. Allied Sci.* **27**, 135–139 (2002).

18. Kendall, E. J. C., Bynoe, M. L. & Tyrrell, D. A. J. Virus isolations from common colds occurring in a residential school. *Br. Med. J.* **2**, 82–86 (1962).

19. Tyrrell, D. A. J. & Bynoe, M. L. Cultivation of a Novel Type of Common-cold Virus in Organ Cultures. *Br. Med. J.* **1**, 1467–1470 (1965).

20. Hoorn, B. & Tyrrell, D. A. J. A new virus cultivated only in organ cultures of human ciliated epithelium. *Arch. Gesamte Virusforsch.* **18**, 210–225 (1966).

21. Corman, V. M. *et al.* Link of a ubiquitous human coronavirus to dromedary camels. *Proc. Natl. Acad. Sci. U. S. A.* **113**, 9864–9 (2016).

22. Holwerda, M. *et al.* Determining the Replication Kinetics and Cellular Tropism of Influenza D Virus on Primary Well-Differentiated Human Airway Epithelial Cells. *Viruses* **11**, (2019).

23. Foxman, E. F. *et al.* Temperature-dependent innate defense against the common cold virus limits viral replication at warm temperature in mouse airway cells. *Proc. Natl. Acad. Sci. U. S. A.* **112**, 827–832 (2015).

24. Zou, L. *et al.* SARS-CoV-2 Viral Load in Upper Respiratory Specimens of Infected Patients. *N. Engl. J. Med.* **382**, 1177–1179 (2020).

25. He, X. *et al.* Temporal dynamics in viral shedding and transmissibility of COVID-19. *Nat. Med.* (2020) doi:10.1038/s41591-020-0869-5.

26. Kindler, E. *et al.* Efficient replication of the novel human betacoronavirus EMC on primary human epithelium highlights its zoonotic potential. *MBio* **4**, (2013).

27. Dijkman, R. *et al.* Isolation and Characterization of Current Human Coronavirus Strains in Primary Human Epithelial Cell Cultures Reveal Differences in Target Cell Tropism. *J. Virol.* **87**, 6081–6090 (2013).

28. Jia, H. P. *et al.* ACE2 Receptor Expression and Severe Acute Respiratory Syndrome Coronavirus Infection Depend on Differentiation of Human Airway Epithelia. *J. Virol.* **79**, 14614–14621 (2005).

29. Bertram, S. *et al.* TMPRSS2 Activates the Human Coronavirus 229E for Cathepsin-Independent Host Cell Entry and Is Expressed in Viral Target Cells in the Respiratory Epithelium. *J. Virol.* **87**, 6150–6160 (2013).

30. Alpern, D. *et al.* BRB-seq: Ultra-affordable high-throughput transcriptomics enabled by bulk RNA barcoding and sequencing. *Genome Biol.* **20**, 71 (2019).

31. Kelly, J. N. *et al.* Comprehensive single cell analysis of pandemic influenza A virus infection in the human airways uncovers cell-type specific host transcriptional signatures relevant for disease progression and pathogenesis. *bioRxiv* 2020.04.03.014282 (2020) doi:10.1101/2020.04.03.014282.

32. Muth, D. *et al.* Attenuation of replication by a 29 nucleotide deletion in SARS-coronavirus acquired during the early stages of human-to-human transmission. *Sci. Rep.* **8**, (2018).

33. Su, Y. C. *et al.* Discovery of a 382-nt deletion during the early evolution of SARS-CoV-2. *bioRxiv* 2020.03.11.987222 (2020) doi:10.1101/2020.03.11.987222.

34. Thao, T. T. N. *et al.* Rapid reconstruction of SARS-CoV-2 using a synthetic genomics platform. *bioRxiv* 2020.02.21.959817 (2020) doi:10.1101/2020.02.21.959817.

35. Frieman, M. *et al.* Severe Acute Respiratory Syndrome Coronavirus ORF6 Antagonizes STAT1 Function by Sequestering Nuclear Import Factors on the Rough Endoplasmic Reticulum/Golgi Membrane. *J. Virol.* **81**, 9812–9824 (2007).

36. Züst, R. *et al.* Coronavirus non-structural protein 1 is a major pathogenicity factor: Implications for the rational design of coronavirus vaccines. *PLoS Pathog.* **3**, 1062–1072 (2007).

37. Kuri, T. *et al.* The ADP-ribose-1″-monophosphatase domains of severe acute respiratory syndrome coronavirus and human coronavirus 229E mediate resistance to antiviral interferon responses. *J. Gen. Virol.* **92**, 1899–1905 (2011).

38. Züst, R. *et al.* Ribose 2'-O-methylation provides a molecular signature for the distinction of self and non-self mRNA dependent on the RNA sensor Mda5. *Nat. Immunol.* **12**, 137–143 (2011).

39. Kindler, E. *et al.* Early endonuclease-mediated evasion of RNA sensing ensures efficient coronavirus replication. *PLoS Pathog.* **13**, (2017).

40. Niemeyer, D. *et al.* The papain-like protease determines a virulence trait that varies among members of the SARS-coronavirus species. *PLoS Pathog.* **14**, (2018).

41. Lokugamage, K. G., Hage, A., Schindewolf, C., Rajsbaum, R. & Menachery, V. D. SARS-CoV-2 is sensitive to type I interferon pretreatment. *bioRxiv* 2020.03.07.982264 (2020) doi:10.1101/2020.03.07.982264.

42. Davidson, S. *et al.* IFN λ is a potent anti-influenza therapeutic without the inflammatory side effects of IFN α treatment . *EMBO Mol. Med.* **8**, 1099–1112 (2016).

43. Galani, I. E. *et al.* Interferon-λ Mediates Non-redundant Front-Line Antiviral Protection against Influenza Virus Infection without Compromising Host Fitness. *Immunity* **46**, 875-890.e6 (2017).

44. Jonsdottir, H. R. & Dijkman, R. Characterization of human coronaviruses on well-differentiated human airway epithelial cell cultures. in *Coronaviruses: Methods and Protocols* 73–87 (Springer New York, 2015). doi:10.1007/978-1-4939-2438-7_8.

45. Thiel, V. *et al.* Mechanisms and enzymes involved in SARS coronavirus genome expression. *J. Gen. Virol.* **84**, 2305–2315 (2003).

46. Lauber, C. *et al.* Transcriptome analysis reveals a classical interferon signature induced by IFNλ4 in human primary cells. *Genes Immun.* **16**, 414–421 (2015).

47. Schindelin, J. *et al.* Fiji: an open-source platform for biological-image analysis. *Nat. Methods* **9**, 676–682 (2012).

48. Mutterer, J. & Zinck, E. Quick-and-clean article figures with FigureJ. *J. Microsc.* **252**, 89–91 (2013).

49. Chen, H. & Boutros, P. C. VennDiagram: a package for the generation of highly-customizable Venn and Euler diagrams in R. *BMC Bioinformatics* **12**, 35 (2011).

50. Yu, G., Wang, L. G., Han, Y. & He, Q. Y. ClusterProfiler: An R package for comparing biological themes among gene clusters. *Omi. A J. Integr. Biol.* **16**, 284–287 (2012).

51. Gu, Z., Eils, R. & Schlesner, M. Complex heatmaps reveal patterns and correlations in multidimensional genomic data. *Bioinformatics* **32**, 2847–2849 (2016).

Figure legends

Figure 1. SARS-CoV and SARS-CoV-2 replication kinetics in hAEC cultures.

Well-differentiated hAEC cultures were infected with SARS-CoV and SARS-CoV-2 using 30,000 PFU or remain uninfected (mock), and were incubated at 37°C (**a, c**) or 33°C (**b, d**). Inoculated virus was removed at 1 hpi and the apical side was washed. Cultures were further incubated at the indicated temperature. At the indicated time post infection, apical virus release was assessed by plaque titration (**a-b**). Data represent the mean ± SEM of three independent experiments. Individual points represent the average of two replicates. Values at 0 hpi indicate the titer of the inoculum used to infect the hAEC cultures. The p-values were computed by using two-sided paired sample t tests, only significant results are shown. At 96 hpi, hAEC cultures were fixed and processed for immunofluorescence analysis using antibodies against SARS-CoV Nucleocapsid protein (green), β-tubulin IV (cilia, red), ZO-1 (tight junctions, white) and DAPI (blue) (**c-d)**. Representative z-projections of one donor are shown. Scale bar, 20 microns.

Figure 2. SARS-CoV and SARS-CoV replication upon IFN-I and IFN-III pretreatment

hAEC cultures were treated from the basolateral side with recombinant universal type I interferon (100 IU/ml) or recombinant IFN-λ3 (100 ng/ml) for 18 h. Before infection, medium was removed and replaced with IFN-free medium and hAEC cultures were infected with SARS-CoV (**a-b, e-f**) and SARS-CoV-2 (**c-d, g-h**) using 30,000 PFU, and were incubated at 37°C (**a, c, e, g**) or 33°C (**b, d, f, h**). Inoculated virus was removed at 1 h.p.i., and the apical side was washed. Cultures were further incubated at the indicated temperature. At the indicated time, apical virus release was assessed by plaque titration (**a-d**). Data represent the mean ± SEM of three independent experiments. Individual points represent the average of two replicates. Values at 0 hpi indicate the titer of the inoculum used to infect the hAEC cultures. The p-values were computed by using two-sided paired sample t tests, only significant results are shown. At 96 hpi, hAEC cultures were fixed and processed for immunofluorescence analysis using antibodies against SARS-CoV Nucleocapsid protein (green), β-tubulin IV (cilia, red), ZO-1 (tight junctions, white) and DAPI (blue) (**e-h**). Representative z-projections of one donor are shown. Scale bar, 20 microns.

Figure 3. Temperature-dependent transcriptional host response in SARS-CoV and SARS-CoV-2 virus-infected hAEC cultures.

Venn diagrams showing the overlap of differential expressed genes (DEG) in SARS-CoV-2 virus-infected hAEC cultures among the different time point and temperature conditions (**a, b**). Hierarchical cluster analysis of DEG identified in SARS-CoV and SARS-CoV-2 virus-infected hAEC cultures, incubated at either 33°C or 37°C. Expression levels – $\log_2$ Fold Change compared to uninfected hAEC cultures – for individual genes are shown in rows and stratified by condition, and hours post-infection (columns; representative colours shown in legends) (**c**). Bar graphs illustrating pathway enrichment analysis performed on 16 different distinct DEG profiles. Enriched pathways displayed on the left (y-axis) are divided by time points. Significant enriched pathways for SARS-CoV-2 are shown for 33°C and 37°C incubation temperature. Bars were adjusted in size and colour to illustrate the fold enrichment and adjusted p-value (< 0.05) for a given pathway, respectively (**d**). Hierarchical cluster analysis of the

expression of 43 genes associated with the detected enriched pathways (**e**). Expression levels (Log_2 fold change) for individual genes are shown in rows and stratified by condition, and hours post-infection (columns; representative colours shown in legends). Bar graphs illustrating the log_2 fold change expression levels over time for IFNL1, IFNL2, IFNL3 and IFNB1, at the respective temperatures for SARS-CoV (top right panels) and SARS-CoV-2 (bottom right panels) virus-infected hAEC cultures. Bars were adjusted in colour to illustrate the respective adjusted p-value (**f**).

Figure 1

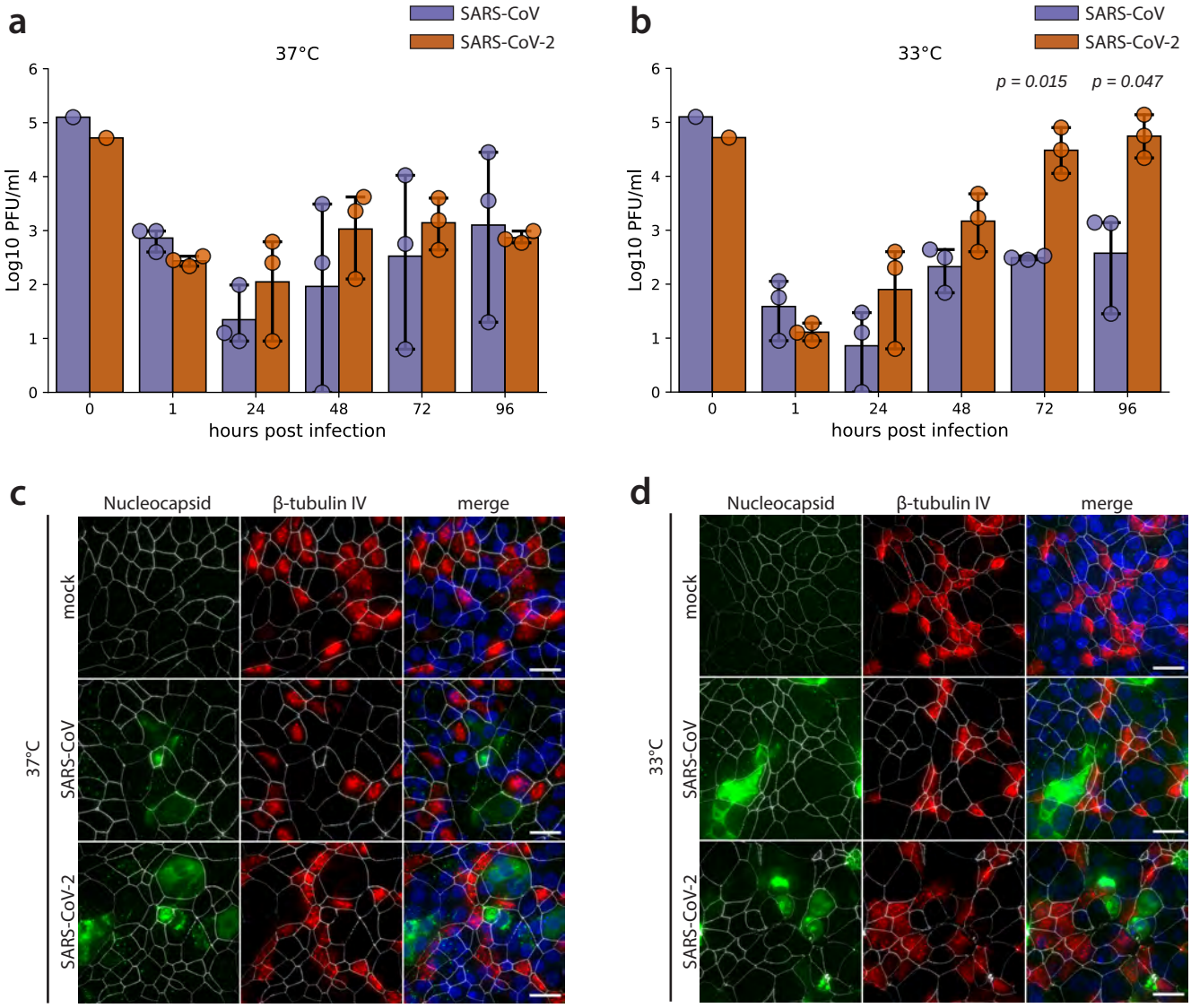

Figure 2

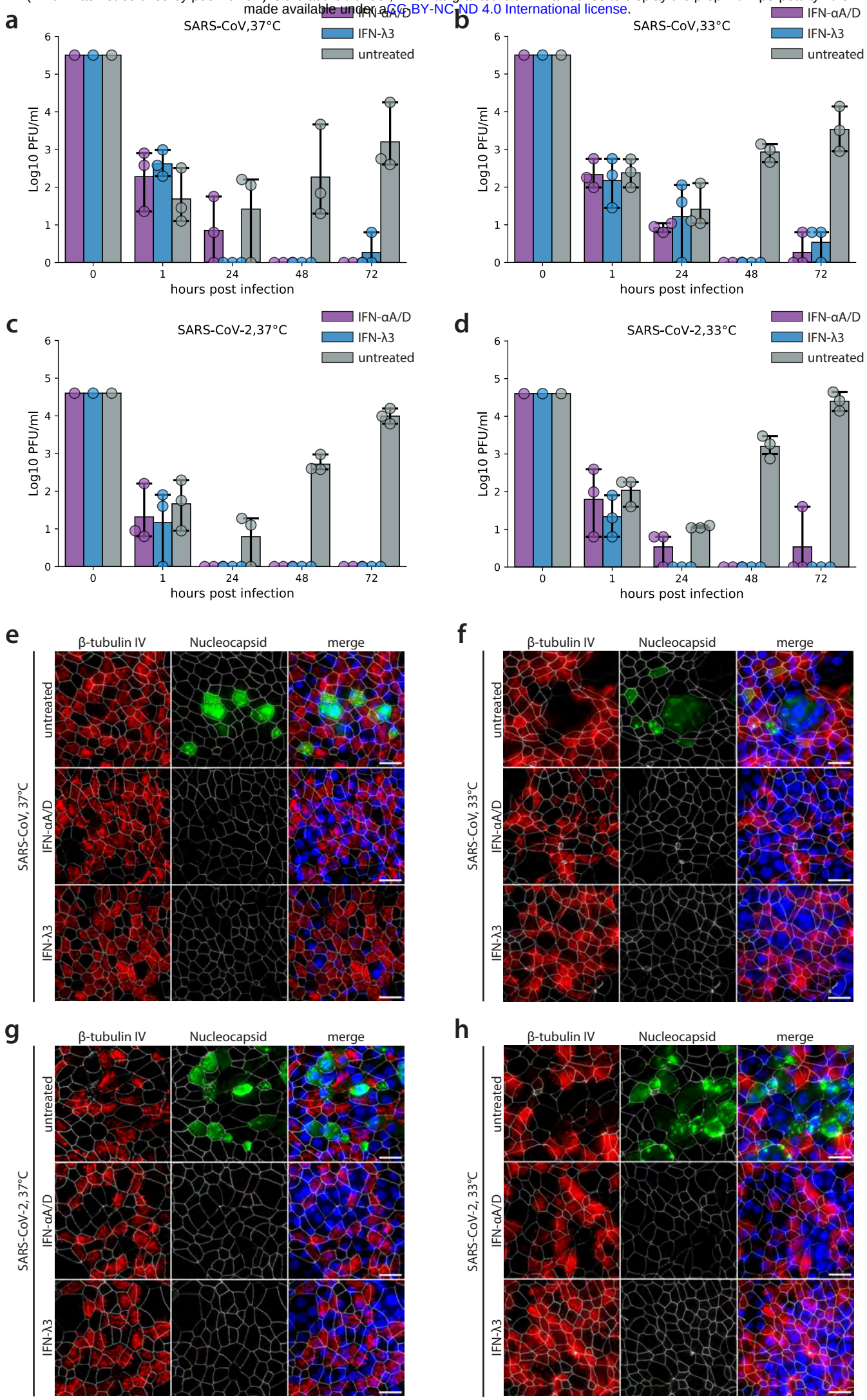

Figure 3